Miniature Heart Cell Force Transducer System Implemented in MEMS Technology

Gisela Lin*, Roy E. Palmer, Kristofer S. J. Pister, and Kenneth P. Roos

***Abstract*—A fully submersible force transducer system for use with isolated heart cells has been implemented using microelectromechanical systems (MEMS) technology. By using integrated circuit fabrication techniques to make mechanical as well as electrical components, the entire low-mass transducer is only a few cubic millimeters in size and is of higher fidelity (≈100 nN and 13.3 kHz in solution) than previously available. When chemically activated, demembranated single cells attached to the device contract and slightly deform a strain gauge whose signal is converted to an amplified electrical output. When integrated with a video microscope, the system is capable of optical determination of contractile protein striation periodicity and simultaneous measurement of heart cell forces in the 100-nN to 50-μN range. The average measured maximal force was $F_{\max} = 5.77 \pm 2.38$ μN. Normalizing for the cell's cross-sectional area, $F_{\max}$/area was 14.7 ± 7.7 mN/mm^2. Oscillatory stiffness data at frequencies up to 1 kHz has also been recorded from relaxed and contracted cells. This novel MEMS force transducer system permits higher fidelity measurements from cardiac myocytes than available from standard macro-sized transducers.**

***Index Terms*—CMOS, force transducer, heart cell, MEMS, micromachining, micromechanical.**

I. Introduction

THE MEASUREMENT of contractile force in the μN range from isolated ventricular heart cells (cardiac myocytes) is crucial to the fundamental understanding of function in normal and diseased heart. The complicated organization of the heart precludes all but the simplest measures of cardiac function. Isolated cardiac myocytes provide a simplified model that can more directly be related to the molecular structures responsible for contraction and its regulation. However, current transducer technology has limited mechanical measurements from cardiac myocytes [1]–[10]. Commercially available force transducers are relatively large and must be placed outside the cell's saline bath. Cell attachment can only be achieved with relatively complex massive structures (e.g.: pipettes, needles, fibers, troughs, plates, or paddles), which are subject to surface tension forces that are likely greater than that of the cell's force [2], [7]. These factors inherently limit "macro" transducer force measurements to frequency ranges of no more than a few hundred hertz.

Microelectromechanical systems (MEMS) technology offers the ability to shrink the entire force transducer down to a size comparable to that of a single heart cell. MEMS uses materials and fabrication techniques derived from integrated circuit technology to create micro-scale machines composed of mechanical components in addition to the traditional electronics [11]. Submersing a miniaturized device into the cell's saline bath increases measurement fidelity and reduces the noise of the system by decreasing attachment arm mass and eliminating the surface tension artifact.

MEMS technology without electronic transduction has been recently applied to evaluate the mechanical characteristics of isolated skeletal muscle myofibrils [12], [13], but full-featured MEMS devices have not been previously employed to evaluate passive or active contractile function in any type of muscle preparation. Recently tungsten needles attached to steel foils were used to record isometric forces and rate constants of force development from isolated cardiac myocytes. Although the force transducer has a resonant frequency in the 2–3 kHz range, the force sensing apparatus is only partially submerged. Also, input mechanical length perturbations are limited to frequencies well below the resonance frequency in order to avoid unstable oscillations [14].

The design of a useful MEMS force transducer must address several criteria to permit the study of mechanical properties of mammalian cardiac myocytes. It is desirable for the device to have a mechanical bandwidth in the kilohertz range so that oscillatory and transient analyses of force can be achieved with high fidelity. The device must also permit a transmitted light path through the cell to visually monitor its ends, attachment integrity, and length during a contraction. Furthermore, the device should exhibit minimal compliance so that the cell length does not change significantly during a contraction unless desired.

This paper describes a miniaturized, fully submersible force transducer system implemented in a technology that satisfies these criteria. Initial prototypes were implemented in polycrystalline silicon ("polysilicon") with a visual deflection readout that was limited by a high beam compliance and finite video image resolution [15], [16]. Therefore, subsequent prototypes implemented in a complementary metal–oxide–semiconductor (CMOS) fabrication process incorporated on-chip strain gauges and amplification electronics to achieve a voltage readout [17], [18]. The design described in this report integrates three-dimensional (3-D) microstructures and signal processing electronics

Manuscript receivedJune 29, 2000; revised June 2, 2001. This work was supported by a Grant-in-Aid from the American Heart Association, Greater Los Angeles Affiliate, under Grants 1059 GI-1, 2, 3 (KSJP). This work was also supported in part by the National Institutes of Health (NIH) under Grant HL-47065 (KPR). *Asterisk indicates corresponding author.*

*G. Lin is with Standard MEMS Incorporated, 7155 Crest Road, Rancho Palos Verdes, CA 90275 USA (e-mail: glin@smems.com).

R. E. Palmer is with Caresoft Incorporated, Sunnyvale, CA 94086 USA.

K. S. J. Pister is with the Berkeley Sensor and Actuator Center (BSAC), University of California, Berkeley, 497 Cory Hall, Berkeley, CA 94720-1770 USA.

K. P. Roos is with the Cardiovascular Research Laboratory, and the Department of Physiology, UCLA School of Medicine, Los Angeles, CA 90095-1760 USA.

Publisher Item Identifier S 0018-9294(01)07442-0.

onto a single chip, $(2\ \text{mm})^3$ in size. A full range of tests has been performed on this low-mass, disposable transducer with and without cardiac myocytes. With this device, direct force and oscillatory stiffness data from relaxed and activated cardiac myocytes exceed the fidelity obtained with standard "macro" transducers and demonstrate the potential for considerably improved mechanical measurements of cardiac myocytes or other cell types using MEMS-based transducers.

II. Theory

A schematic diagram of the MEMS force transducer system is shown in Fig. 1. The heart cell ends are attached to the transducer beams using silicon dioxide ("oxide") clamps. One of these oxide beams incorporates a strain gauge made of polysilicon, which is a piezoresistive material changing resistance when mechanically deformed. Thus, when the cell contracts, the sensor beam bends, activating the strain gauge; the opposite beam is immobilized. The strain gauge serves as the variable resistor in an on-chip Wheatstone bridge. The bridge converts the change in strain gauge resistance into a change in voltage which is then amplified on-chip for recording off-chip.

Force in muscle cells is generated by the interaction between the contractile proteins, actin and myosin, which form a molecular motor. They are organized within sarcomere units of parallel contractile filaments that are visible as cross-striations in an optical microscope (see Fig. 10) [19]. Although the maximal force from individual molecular motors is approximately the same within a given muscle, the maximal force from different heart cells is variable depending upon the number of force generators in cross-section [2], [7], [8]. Thus, in order to relate mechanical data from cells of different sizes to their fundamental molecular source, measured force must be normalized to the cross-sectional area of the cell. As an approximation, the myocyte cross section was estimated as an ellipse with a major axis to minor axis ratio of 1.25 : 1 [8]. The area of the cell cross section was then

$$A = \left(\frac{1}{1.25}\right)\pi\left(\frac{w}{2}\right)^2 \tag{1}$$

where w is the measured width of the cell's major axis.

In terms of the device characteristics, various parameters of the transducer system can be theoretically estimated. For example, the spring constant of a single fixed-free cantilever beam is described by [20]

$$k(a, b, L) = \frac{a^3 bE}{4L^3} \tag{2}$$

where

- a beam thickness $= 3.05\ \mu$m;
- b beam width $= 20\ \mu$m;
- L beam length $= 100\ \mu$m;
- E elastic modulus of silicon dioxide $= 0.73 \times 10^{11}$ Pa [21].

Theoretically, the spring constant of this single fixed-free oxide cantilever beam is 10 N/m.

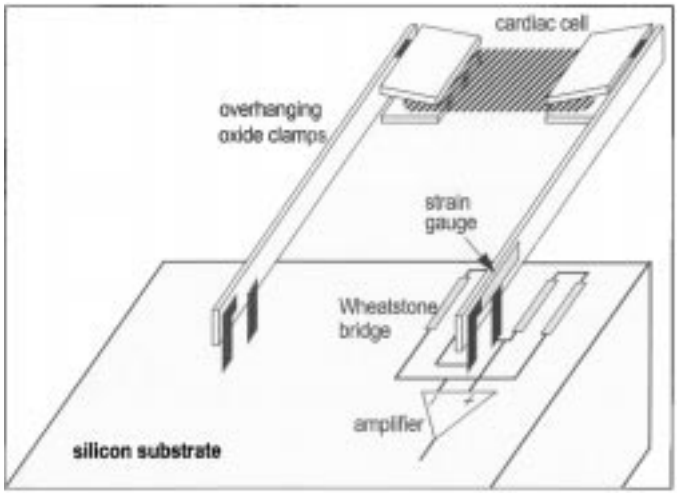

Fig. 1. Schematic diagram of the force transducer system. See the text for details on its principle of operation.

The equation of motion describing a damped oscillator with no external force acting on the oscillator once it is in motion is [22], [23]

$$\frac{d^2x}{dt} + 2\zeta\omega_n\frac{dx}{dt} + \omega_n^2 x = 0 \tag{3}$$

where $\omega_n =$ the natural undamped angular frequency and $\zeta =$ the damping ratio described by

$$\zeta = \sqrt{1 - \left(\frac{\omega_d}{\omega_n}\right)^2} \tag{4}$$

where $\omega_d =$ measured, damped frequency. The on-chip system response is determined by starting with the theoretical response of a Wheatstone bridge with one variable resistor from basic mechanics, circuit theory, and models for piezoresistance [20], [24], [25]

$$\frac{dV_{\text{bridge}}}{dF} = \frac{3V_{\text{in}}GL}{2a^2bE} \tag{5}$$

where

- V_{bridge} output voltage of the bridge;
- V_{in} input voltage driving the bridge;
- F input force that deforms the piezoresistor (variable resistor);
- G gauge factor of the polysilicon piezoresistor;
- a beam thickness;
- b beam width;
- L beam length;
- E elastic modulus of the oxide beam.

For design purposes, a gauge factor of -20 was used, meaning a 1% change in strain produces a 20% change in resistance. Thus, with 1 V driving the bridge, the theoretical bridge response is 0.22 mV/μN. Multiplying by the gain of the on-chip amplifier (in this case 12), the predicted on-chip system response is 2.6 mV/μN.

The threshold of force resolution (device sensitivity) is determined by the noise level in the system. Noise produced by

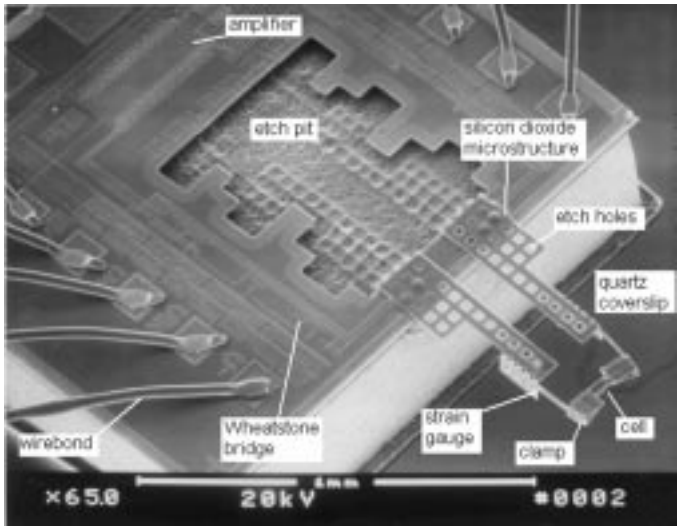

Fig. 2. SEM photo of the device, without encapsulation. The microstructure on a quartz coverslip is flipped over the edge of the wafer revealing the cavity left behind after etching. In this photo, a fixed (dried) heart cell is glued between the oxide clamps. The base of the lower beam contains a piezoresistive strain gauge connected to the Wheatstone bridge circuit via the aluminum hinges. Gold wirebonds transfer the electrical signals on and off the chip.

the on-chip electronics can be theoretically estimated by simulating these components with a simulation program with integrated circuit emphasis (SPICE) which considers both flicker $(1/f)$ and thermal (Johnson) noise [26]. SPICE estimated the noise variance to be 20 μV. Thus, the on-chip "noise envelope" is 0.12 mV, assuming the envelope is three variances wide on either side of the signal. These estimates are conservative in terms of the actual noise that will be measured since there are other sources of noise that are not accounted for, such as burst noise and noise generated in the device package. However, dividing by the theoretical on-chip system response (2.6 mV/μN), the noise envelope corresponds to a theoretical minimum resolvable force of 46 nN.

III. Methods

A. Device Fabrication

Devices were batch fabricated using a commercial CMOS process [27]. In this process, thin films of polysilicon, oxide, and metals are grown or deposited on a silicon substrate that can also be selectively implanted with ions to locally alter the electrical properties. Both mechanical and electrical components are created by strategically patterning the thin films and ion-implanted areas of the substrate via photolithography and chemical etching. The patterned layers and substrate are connected at specific sites to form electrical interconnect pathways, resistors, strain gauges, and transistors.

The individual devices on the chip are physically separated via wafer dicing. A single device, about 2 mm $\times$ 2 mm in size, is then attached to a quartz coverslip [0.86 in $\times$ 0.86 in $\times$ 0.01 in (Dell Optics, Inc., Fairview, NJ)] using 5-min epoxy. This coverslip had ten aluminum lines previously patterned on it via photolithography and E-beam aluminum evaporation. The chip was wirebonded directly down to these lines providing ten electrical signals to and from the device (see Fig. 5). Fig. 2 shows an SEM

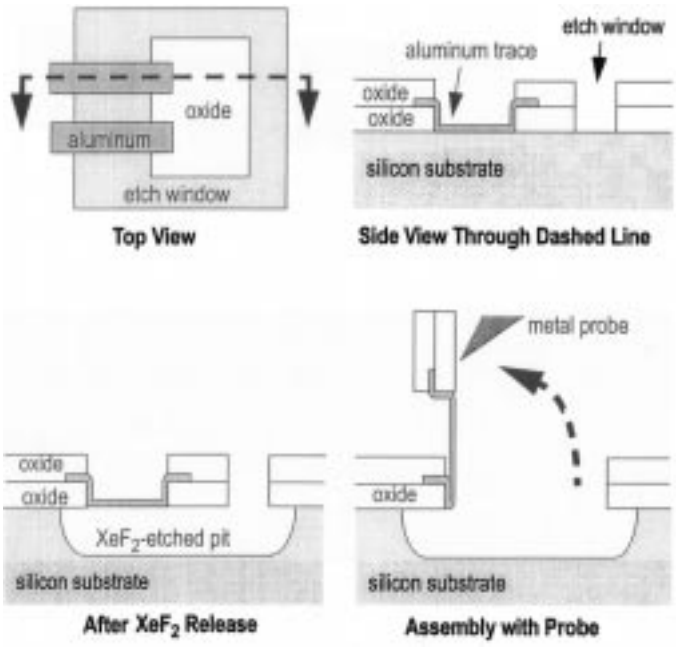

(a)

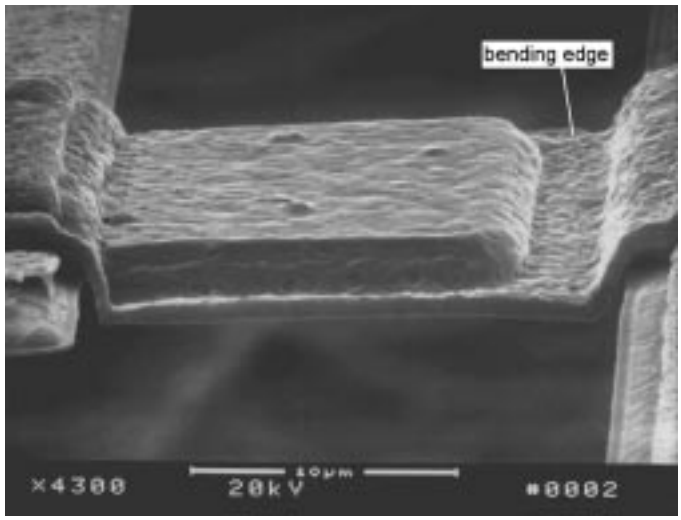

(b)

Fig. 3. Aluminum hinges. (a) Schematic diagram of the fabrication and assembly of an aluminum hinge. Aluminum traces are patterned through an etch window which is exposed silicon substrate. XeF_2 etchant undercuts the oxide plates and aluminum traces. Hinge assembly involves bending the aluminum by lifting the attached oxide pad with a probe. (b) SEM photo of an unassembled, double layered aluminum hinge.

micrograph of the MEMS force transducer system including a Wheatstone bridge, amplifier, cantilevered beams, strain gauge, cell, clamps, and the wires for input power and output signals. Since the silicon substrate of the chip base is opaque, the beam-clamp assemblies are cantilevered off the side of the substrate to permit transmitted light to pass through the cell for imaging.

B. Release Etching

Following device preparation, the mechanical microstructure of the device is freed for assembly by "release etching" the silicon substrate. The etchant, XeF_2, will preferentially etch silicon and polysilicon layers over the oxide and aluminum layers under vacuum conditions. Thus, polysilicon strain gauges are

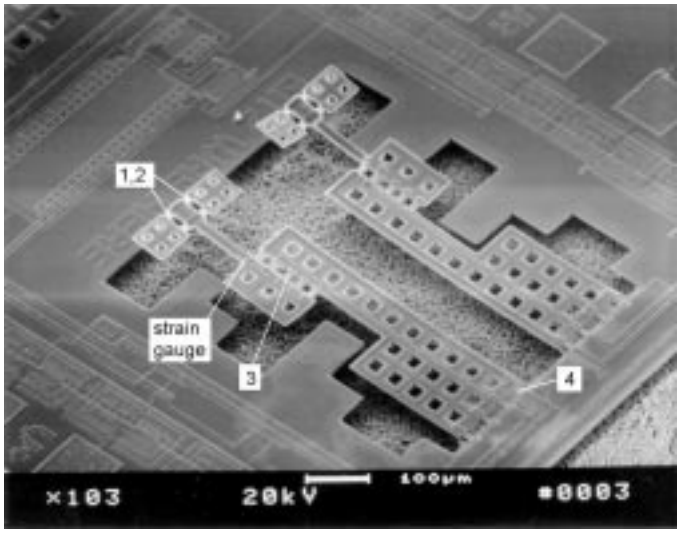

(a)

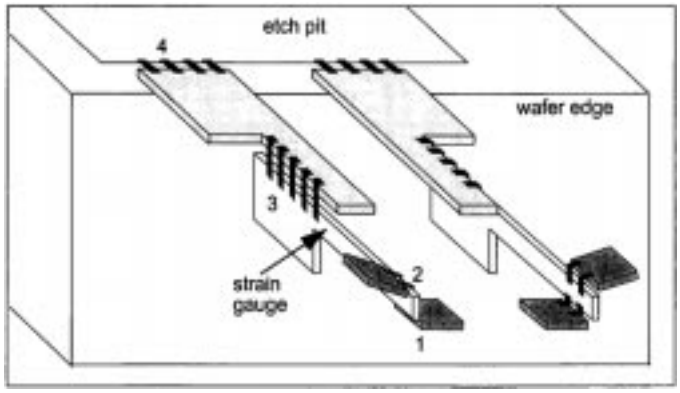

(b)

Fig. 4. Illustration of clamp assembly sequence. (a) SEM of the structure before assembly, immediately after XeF_2 release. (b) Diagram of the structure after assembly, but before cell attachment. The four groups of aluminum hinges on one of the arms are numbered in both (a) and (b).

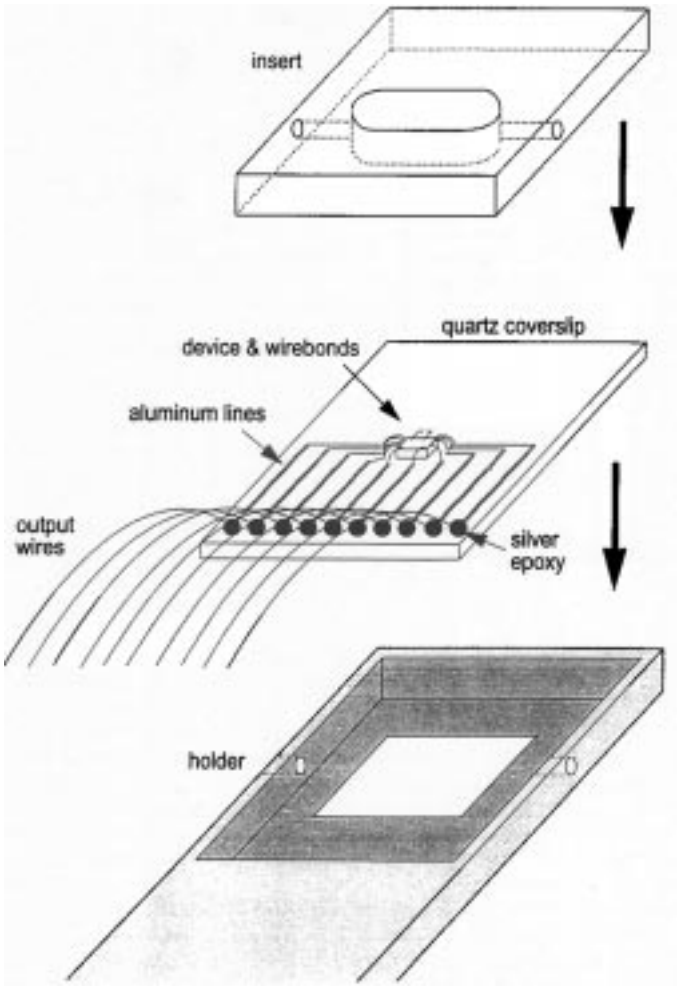

Fig. 5. Diagram of the holder and insert used with the transducer during cell experiments. The insert is placed in the chamber only after successful completion of cell attachment. See the text for details.

preserved if completely encased in the appropriate thickness of oxide. An array of 20 × 20 μm "etch holes" allowed the etchant access to the silicon substrate underneath leaving a scalloped etch "pit" after release (Fig. 2). The microstructure release method and apparatus are detailed by Chu, *et al.* [28].

C. Hinge Fabrication

To make a 3-D MEMS microstructure with cantilevered beams and clamps, simple hinges (Fig. 3) were created from the metal layers [29]. Device assembly involved bending freestanding aluminum beams by lifting the oxide pads with a probe [Fig. 3(a)]. This aluminum beam functions as a hinge by remaining deformed after bending and leaving the oxide pad vertical to the substrate. To prevent microstructure misalignment, hinges are forced to bend along predetermined edges by patterning a first layer of aluminum underneath a portion of a second layer of aluminum. With this double-metal hinge approach [Fig. 3(b)], the first metal layer only extends partially through the hinge, stiffening one edge relative to the other. The aluminum hinges can also function as electrical pathways.

D. Microstructure Assembly and Device Packaging

All microstructure assembly was done manually using four sharp tungsten needle probes (Cascade Microtech Inc., Irvine, CA) and an optical microscope mounted on a Wentworth probe station (Wentworth Laboratories, Brookfield, CT). Fig. 4(a) shows the structure immediately following release etching, but prior to assembly. The hinges are numbered on one side. To assemble the microstructure, hinges #1, #2, and #3 were folded 90° while hinges #4 were folded 180° to flip the entire microstructure off the edge of the wafer [Fig. 4(b)]. The top flaps (60 × 65 μm) of the clamps were folded outwards at hinge #2 to facilitate cell attachment. The beams (from #2 to #3) are 100 × 20 × 3.05μm. Hinges #3 and #4 also served as electrical interconnects to the strain gauge. Specific parts of the device are coated using 5-min epoxy, silicone rubber, and nail enamel for electrical isolation. Following encapsulation, output wires were attached along one edge of the quartz coverslip (Fig. 5) using conductive silver epoxy (Epo-Tek H20E Conductive silver epoxy, Epoxy Technology Inc., Billerica, MA).

E. Experimental Chamber Design

The experimental chamber consisting of a coverslip holder and insert was machined out of acrylic (Fig. 5). The insert has a

small oval chamber ($2.5 \times 7 \times 1.5$ mm) holding about 26 μl of liquid with solution exchange ports at each end. It was designed so that the output wires emerge out one side of the chamber. Vacuum grease (Dow Corning silicone stopcock grease, Midland, MI) was applied to function as a barrier to fluid leakage and secure the coverslip to the inner surface of the holder.

F. Heart Cell and Solution Preparation

Cardiac myocytes were prepared fresh each experimental day from adult rat ventricles subject to retrograde coronary artery perfusion (Langendorff) with 0.1% collagenase (Worthington Biochemical Corp., Freehold, NJ, type 2) in Joklik minimum essential medium (Irvine Scientific, Irvine, CA) at pH 7.4 [6]–[8]. Following 10–20 min of perfusion, the cells were isolated by mincing and mechanically agitating the left ventricle in relaxing solution [6]. These cells were demembranated (skinned) for experiments by adding 1% ultrapure Triton X-100 detergent to the relaxing solution for 20 min. The cells were washed to remove any traces of detergent and attachment to the transducer immediately followed. All cells were used within the first four hours after extraction to eliminate any possible cellular deterioration.

The contractile level of the demembranated (skinned) heart cells was precisely controlled for these experiments using relaxing and activating solutions previously detailed [6]. The cells were maintained for all experiments in relaxing solution at pH 7.4 and pCa ≈ 8. To make the maximal activating solution (pCa $= 4.5$), premixed 0.1M $CaCl_2$ standard (CIBA-Corning Diagnostic Corp, Medfield, MA) was added to relaxing solution in the ratio 1 : 10. Intermediate pCa levels were formulated by proportional mixing of the relaxing and maximal activating solutions. All chemical components used in solutions for cell preparation and the experiments were purchased from Sigma Chemical Company (St. Louis, MO) unless otherwise noted.

G. Cell Attachment

Fig. 6 illustrates the steps for cell attachment. Starting with the device in the holder and the clamp plates open [Fig. 4(b)], silicone sealant was applied to each plate surface using a needle probe [Fig. 6(a), step 1]. Then cells in relaxing solution were introduced into the chamber. A cell of appropriate length was chosen and mounted between the clamps [Fig. 6(a), step 2]. The top plates were rotated to close down upon the cell ends [Fig. 6(a), step 3]. Since the microstructure is very delicate, a small coverglass is used to support the bottom plates to facilitate attachment without beam or clamp breakage.

Fig. 6(b) is a SEM photo of the device after the cell attachment. For this micrograph, the device is not encapsulated, the cell is fixed, and the numbered hinges correspond to those in Fig. 4. After cell attachment, the insert (Fig. 5) was placed in the chamber. The holder with the complete transducer and cell was transferred to the imaging system for data acquisition. These devices are designed for one time use only since they are encapsulated and the living cells irreversibly glued to the clamps.

H. Test Setup and Imaging System

Cell experiments were conducted using a microscope and video imaging system mounted on an air-suspension table. The

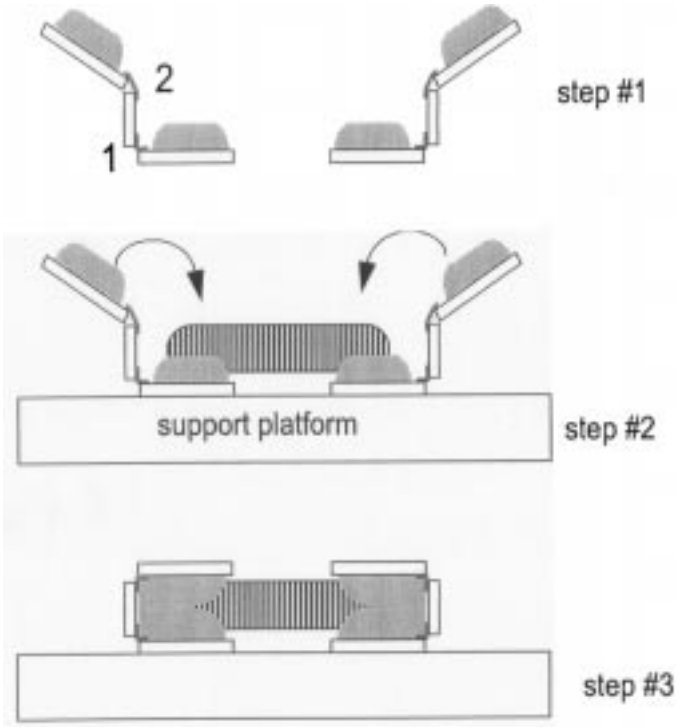

(a)

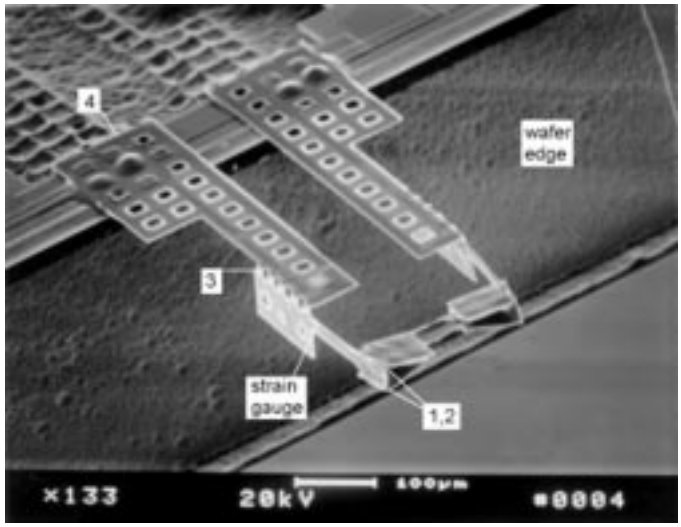

(b)

Fig. 6. Cell attachment steps. (a) The attachment procedure starts with applying glue to the open clamps (step 1). Then a cell of appropriate length is placed between the clamps (step 2) with the aid of a support platform. Finally, the clamps are closed around the cell ends (step 3). (b) SEM of the device after the cell is attached. The hinge numbers correspond to those in Fig. 4.

holder with the device, insert, and cell was bolted down to a two-axis micromanipulator (Melles Griot, Irvine, CA) for X–Y positioning over the optical axis of an inverted water immersion 40 X microscope objective lens (Zeiss, Germany) as shown in Fig. 7. Z-axis objective positioning with a third micromanipulator provided focus. A light emitting diode positioned above the experimental chamber transilluminated the cell and transducer arms. Video image data were visualized on a monitor and recorded on tape or laser disk for later analysis [30].

Following the attachment procedure, the cell was usually slack between the clamps due to the difficulty of attaching a

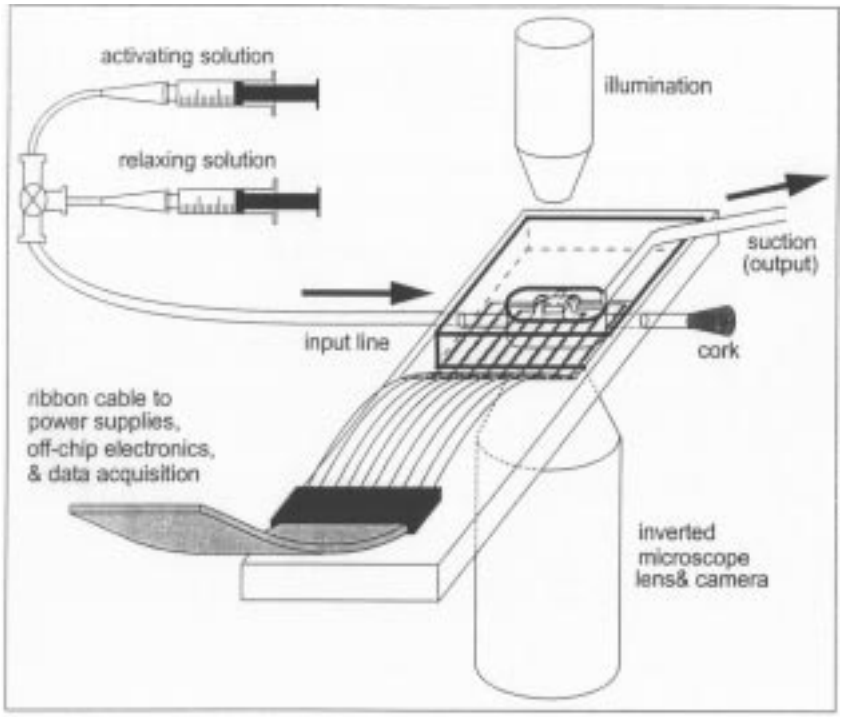

Fig. 7. Schematic diagram of the experimental setup. The holder sits on top of an inverted microscope lens with camera underneath to image the cell. Bathing solutions are pumped in manually through the input line and out via a suction tube placed at the top of the chamber. The suction tube also controls the level of the solution meniscus. Output wires emerge from underneath the insert to interface with power supplies, off-chip electronics, and the data acquisition system. The array of tungsten needle probes (each attached to a three-axis micromanipulator mounted around the experimental chamber) is not shown for simplicity.

cell during the assembly process. Since this is not the normal condition in the heart [2], [7], it was necessary to remove any slack by moving the clamps further apart. Thus, after installation on the microscope system, an external needle probe was inserted into the clamp opposite the arm with the strain gauge. This crude method not only took up the slack and stretched the cell to an appropriate length, but it also immobilized this end. Hence, the entire force was sensed by the arm containing the strain gauge.

Activating and relaxing solutions were manually pumped through the input line into the chamber (Fig. 7). A glass suction tube was placed at the top of the chamber to remove excess fluid and maintain a constant solution meniscus level for a steady focus of the cell image during solution changes [6].

I. Image Analysis

Stored video image data were digitized using a PC-based frame-grabber system. These data were subsequently filtered, contrast-enhanced, and analyzed to obtain cell length (transducer clamp spacing) and sarcomere striation pattern periodicity using custom software [30]. At the relatively low magnification used for these studies, the system had a spatial resolution of approximately 5 pixels/μm (± 0.20 μm). Both the cell length and sarcomere striation periodicity (sarcomere length) were continuously measured during each experiment.

J. Force Measurements and Signal Processing

To obtain a usable voltage signal representing cell force from the transducer arm deflection, the signal changes from the Wheatstone bridge needed to be amplified and processed on and off the chip (Fig. 8). Since functional integration of the on-chip electronics, the folded microstructure, and the interconnect hinges was a major goal in device development, the on-chip electronics were kept extremely simple. The on-chip amplifier is composed of nine transistors (differential input stage, biasing transistors, and output stage). Due to the lack of a gain stage, the on-chip gain was very low (12) and additional gain was needed. A low-noise operational amplifier (MAX427, Maxim Integrated Products, Sunnyvale, CA) and a simple resistor and capacitor filter were added off-chip. The off-chip electronics were configured to have a maximum gain of 511 and a filter roll off at 7.2 Hz to achieve a measurable change in output voltage. However, the gain and roll-off could be easily adjusted by changing the resistors R1 and R2, respectively (see Fig. 8).

The Wheatstone bridge was biased from -0.3 V to -1.3 V, and the on-chip amplifier was biased from 3.2 V to -6.8 V. These biasing rails were chosen to achieve an on chip signal centered at ≈ 0 V to utilize the full dynamic range of the off-chip electronics. For the transducer evaluations with attached cells, the off-chip gain was typically reduced to 325 so that the output signal would remain within the ± 5 V input range of the data acquisition system. All signals were recorded for analysis with either a digital oscilloscope (HP 54 600B, Palo Alto, CA) or with a computer equipped with a LabVIEW data acquisition and control system (National Instruments, Austin, TX).

Prior to a contraction experiment, beam displacement versus output voltage (V_{out}) was recorded for each device by manually deflecting the sensor beam using a separate probe and measuring the change in output voltage in air (without cell) and solution (with cell in the clamps) [18]. Even though the cell is

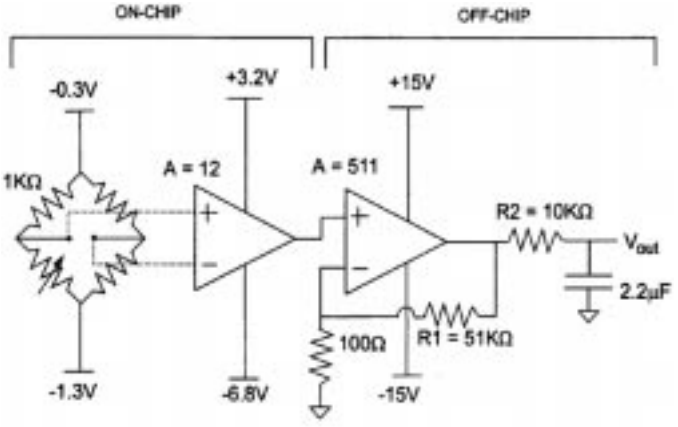

Fig. 8. Schematic diagram of the on-chip and off-chip electronics. The indicated bias voltages were used to center the output voltage to around 0 V, allowing optimal use of the system's dynamic range during data acquisition.

present, it had no effect upon this type of "on-site calibration." Using these data and the calibrated spring constant of the beam, $V_{\rm out}$ could be directly correlated to force.

K. System Response and Beam Calibration

The beam containing the piezoresisitive polysilicon strain gauge (Figs. 2 and 6) was calibrated using a standard "macro" force transducer, the Cambridge 406A (Cambridge Technologies, Watertown, MA 02172) [6], [8], [9]. The Cambridge transducer was used to apply a known force to the beam by directly interfacing its glass tip to the end of the MEMS transducer beam. The change in output voltage of both the Cambridge and the MEMS force transducers was recorded simultaneously for various amounts of applied force. The Cambridge force transducer was calibrated separately by hanging wires of known weights off the force transducer. Its response was 13 mV/μN and was linear [6]. The change in Cambridge output voltage was then converted to applied force and plotted versus the corresponding change produced in the MEMS system output voltage to determine the MEMS system response. In a separate experiment, the MEMS beam was deflected with a probe in air, and the corresponding change in output voltage $(V_{\rm out})$ was recorded. By dividing the slope of the best-fit line in the $\Delta V_{\rm out}$ versus deflection curve by the slope of the $\Delta V_{\rm out}$ versus force curve, an estimate of the beam's spring constant for each device was obtained.

L. Mechanical Bandwidth Measurements

To determine the beam's mechanical bandwidth, it was deflected approximately 10 μm and quickly released. The deflection was achieved using a needle probe attached to an external piezoelectric disk (Radio Shack, #273-091B, Ft. Worth, TX 76102). The beam was released when a programmed step voltage delivered to the piezoelectric disk caused the needle to quickly move to the side and cleanly disengage. This action allowed the beam to "flick" back to its normal position with a resulting oscillation. The MEMS system output response was recorded using a digital oscilloscope.

M. Oscillatory Data

To perform the oscillation experiments with attached cells, the needle probe from the piezoelectric disk was inserted into the clamp opposite the sensor beam (instead of the manual length adjustment probe used in the maximal force study). Using the digital oscilloscope to record the MEMS system output response, sinusoids of various frequencies and of a few microns in longitudinal displacement (1%–2% cell length) were delivered to perturb the cell. The off-chip gain was set to 511, and the roll-off of the filter electronics (Fig. 8) was changed to 1800 Hz. Then, steady state "snapshots" were taken at frequencies ranging from 10 Hz to 1800 Hz under both relaxing and activating conditions. Though separate tests revealed nonlinearities in the piezoelectric disk's frequency characteristics, it was deemed acceptable for preliminary cell oscillation experiments up to 1.8 KHz.

IV. Results

A. Transducer Characteristics

Averaging over eight devices, the measured MEMS system response was 0.81 $\pm$ 0.16 V/μN. Dividing by the gain of the off-chip amplifier (511), the on-chip system response was 1.6 $\pm$ 0.31 mV/μN. Averaging over eight devices, the calibrated spring constant of the beam was 2.8 $\pm$ 0.42 N/m. In general, the system response was linear with a small amount of scatter that can be attributed to a variety of sources. One potential source was slippage or variation in contact interface between the polished and rounded Cambridge glass pipette tip and the MEMS beam. Other sources of scatter could arise from electronic noise or temperature sensitive variations in either transducer system.

The unfiltered output responses of the mechanical bandwidth tests in air and water are shown in Fig. 9(a) and (b). The mechanical bandwidth estimated from the cycle time of the oscillations (f_d) was approximately 30.3 KHz in air and 13.3 KHz in water. The natural frequencies (f_n) were 30.3 KHz in air and 13.7 KHz in water (via nonlinear curve fitting of the data in Fig. 9). The corresponding damping ratios [by (4)] were 0.0081 in air and 0.24 in water. These levels of damping are negligible, indicating that the beam is close to resonating in both environments under these experimental conditions.

The damping force can be derived from the analytical values of mass, f_n, and ζ in air and water along with the velocity of the beam. From the data in Fig. 9, the beam velocity was estimated to be 0.17 m/s in air and 0.031 m/s in water. The damping force is described by the second term in (3), and the values inferred from these data are 46 nN in air and 500 nN in water. Since a heart cell's shortening velocity is less than the speed of the beam in this test ($\approx$0.008 m/s), the damping force it experiences is about $\approx$100 nN. Compared with the micronewton forces expected from the cells, this level of damping force should not hinder clamp and beam movement through the saline bath.

The measured output noise of the whole device was typically 0.1 V peak-to-peak. Dividing by the off-chip gain (511 for these tests) and ignoring the off-chip noise, the measured on-chip "noise envelope" is 0.2 mV. Dividing by the measured on-chip system response, the analytical minimum resolvable force is roughly 100 nN. With an off-chip gain reduction to 325 (i.e., the

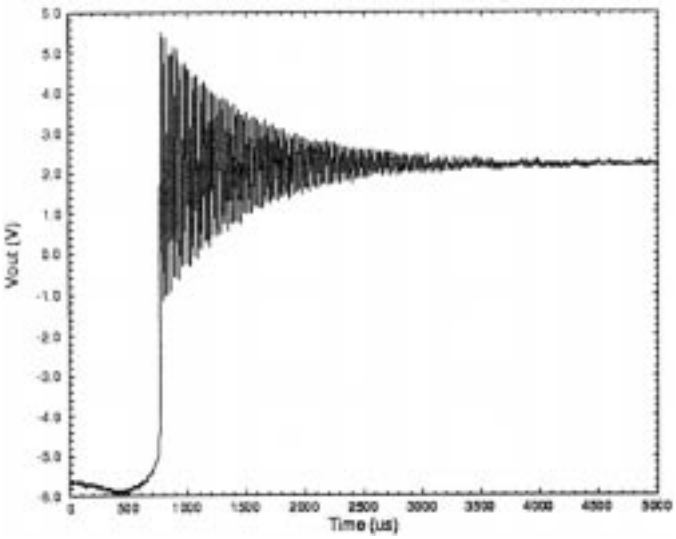

(a)

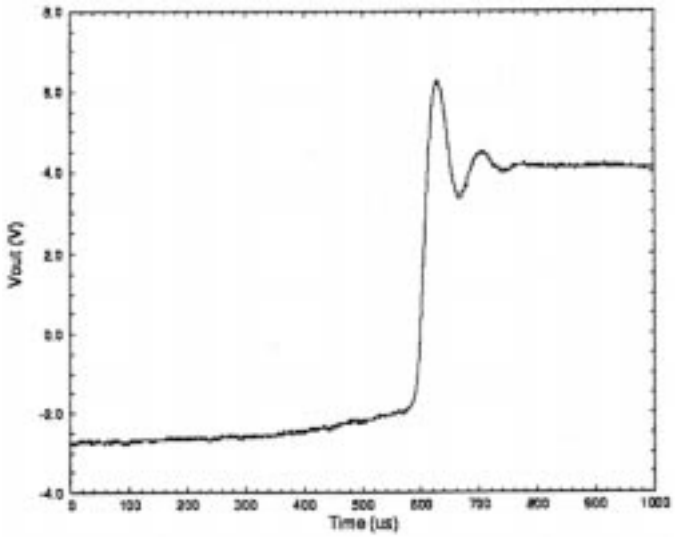

(b)

Fig. 9. Step response of the beam in (a) air and (b) water. See the text for details.

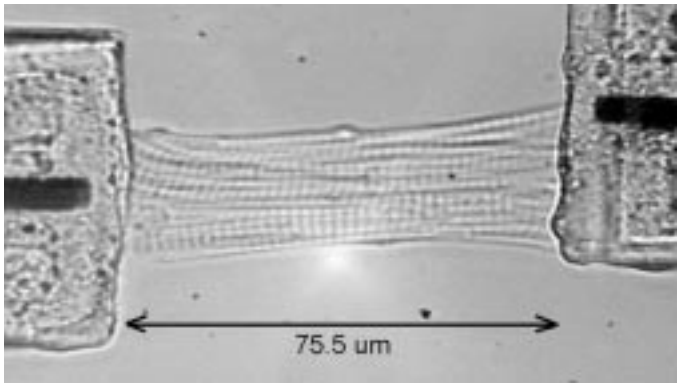

(a)

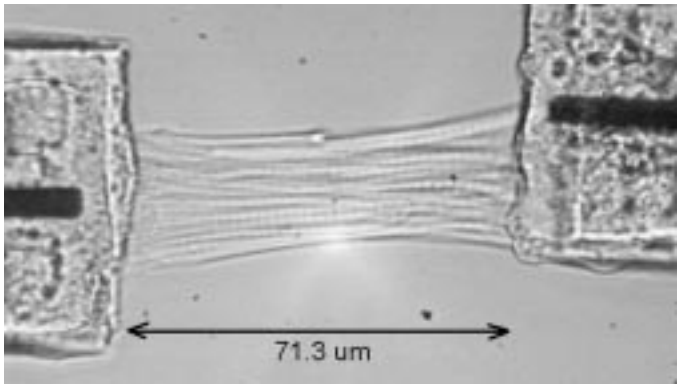

(b)

Fig. 10. Images of attached cell. (a) Attached cell in relaxing solution, clearly showing the sarcomere striation pattern. (b) Same cell during maximal activation showing a less distinct striation pattern and cell shortening. A probe is inserted in the left clamp (not shown) to immobilize that beam and take up cell slack. The force sensor is on the right side.

off-chip gain used for cellular force measurements), the system noise level was about 0.2-V peak-to-peak and corresponded to a 180-nN force floor. This is comparable to the minimal resolvable force attainable through commercial force transducers such as the Cambridge 406A when attached to cells [6].

B. Maximal Force Measurements

Chemically skinned cardiac myocytes were attached to the clamps of this device and their forces measured under controlled steady state and oscillatory conditions. Fig. 10 shows a digitized video image of an attached cell at rest and at the peak of a chemically activated contraction. The optical system permitted imaging of the attachment clamps for cell length determination and the sarcomere striation pattern for sarcomere length determination.

Force development data was recorded from eight skinned cardiac myocytes. Fig. 11 illustrates a complete activation–relaxation sequence from the cell shown in Fig. 10. At point A, infusion of the activating solution (pCa $= 4.5$) was initiated. The spike corresponds to the initial burst of fluid on the transducer beam. After a 4-s delay due to solution transit time and chamber mixing, the cell contracted, developed force, and the transducer output voltage rose. Activating solution was continuously infused into the chamber until point B (Fig. 11). The relatively flat nature of the plateau segment demonstrates the system's minimal noise and drift and the effectiveness of the fluid exchange system. The output voltage dropped slightly at point B because fluid inflow was stopped during this period. The force transient at point C (Fig. 11) corresponds to the resumption of fluid flow with relaxing solution. After another 4-s delay, the cell relaxed and the output voltage returned to its starting position. The small force spike just prior to the relaxation was a consistent feature in these studies. The exact cause of this spike is unclear, but it could be due to some solution mixing issue or the initial phase of relaxation eliciting some degree of cell elongation to a more forceful level along the ascending limb of the force-length relationship. Based on the DC level shift in the trace in Fig. 11, the calibrated maximal force generated by the cell was 9.8 μN. The average $F_{\max}$ over 15 trials on eight cells was 5.77 ± 2.38 μN.

The measured width of each cell was taken to be the major axis of the ellipse for this calculation. Using (1), the average value obtained for $F_{\max}$/area was 14.7 ± 7.68 mN/mm^2. Image analysis determined that the average sarcomere length was 1.99 $\pm$ 0.13 μm at rest and 1.39 $\pm$ 0.16 μm at maximal contraction.

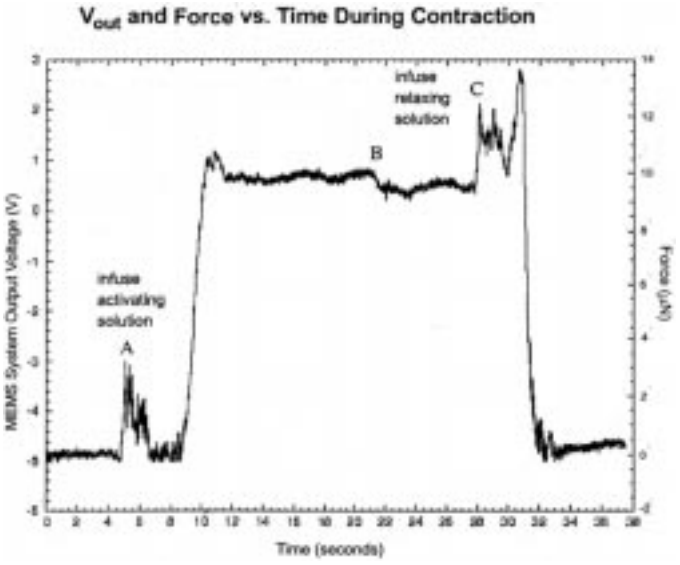

Fig. 11. Force data obtained from cell shown in Fig. 10. From the left prior to point A, the cell is relaxed. At point A, the infusion of activation solution (pCa = 4.5) is initiated. After about 4 s, the force rises rapidly to a plateau. Infusion ceases at point B while the stopcock is switched to relaxing solution. Reinfusion starts at point C. Relaxation follows in about 4 s with the force rapidly returning to a stable baseline level.

C. Cell Oscillation Experiments

Cells were longitudinally oscillated at frequencies ranging from 10 Hz to 1800 Hz. Fig. 12 shows snapshots of such data from relaxed and fully activated cells oscillated at 1 KHz. The qualitative differences in the magnitude of the output trace deflections indicate that the fully activated cell was about 15–20 times stiffer than under the relaxed condition. At lower frequencies, the contracted cell produced force output waveforms that were periodic from 10 Hz to 100 Hz and then consistently sinusoidal from 100 Hz–1800 Hz, while those of the relaxed cell were very noisy at frequencies from 10 Hz to 100 Hz, then roughly sinusoidal from 100 Hz to 1800 Hz.

V. Discussion

The measured on-chip system response was less than that predicted by theory (1.6 ± 0.31 mV/μN versus 2.6 mV/μN). This discrepancy most likely arose from the nonrigid beam support structure that has flexibility. Theory assumes that the beam support is completely rigid. The calibrated beam spring constant was also less than that predicted by theory (2.8 ± 0.42 N/m versus 10 N/m). The difference may arise from the fact that the actual beam consists of multiple layers of four different oxides and a piezoresistor at the base, which would likely function differently than a slab of pure silicon dioxide as assumed in the theoretical estimate. In addition to the nonrigid beam support, this may also explain the discrepancy between theoretical and measured system response as well as the variability in system response.

The estimated mass of the beam and clamp is 8.6×10^{-11} Kg, assuming the beam is composed of a single slab of oxide and the density of oxide is 2.5 g/cm^3 [31]. Using the calibrated spring constant (2.8 N/m) and the mass, the expected mechanical bandwidth is 28.7 KHz, which is close to the experimental result in air. Theoretically the natural frequency should not change with environment. Assuming the spring constant is independent of environment, the analytical results indicate that the mass of the structure has increased by a factor of 4.4 in water. This is analogous to having a boundary layer of water 13 μm thick completely surrounding the beam and clamp. Presumably this boundary layer of water is effectively contributing added mass to the microstructure, which decreases the resonant frequency.

The measured on-chip noise envelope (0.2 mV) is larger than theory predicts (0.12 mV), as expected. However, this value is sufficiently low being less than 1% of the expected maximal forces generated by typical cardiac myocytes (0.2 mV corresponds to a minimum resolvable force $\approx$100 nN via the measured on-chip system response). Also, this indicates that a large portion of the output noise comes from the low-frequency noise in the on-chip electronics, as the theoretical SPICE simulations modeled Johnson and $1/f$ noise in the on-chip electronics. Other sources of noise may include contributions from the packaging or the random thermal cooling effects of the solution environment that surrounds the strain gauge.

The measurements of absolute and normalized forces in cardiac myocytes are slightly less than, but comparable to those found by our own and other groups studying steady-state contractile characteristics of cardiac cells [1], [2], [4], [6], [10]. This discrepancy can be largely attributed to several factors. First, there was a greater MEMS beam compliance than anticipated which permitted cell shortening to less optimal sarcomere lengths. At these very short sarcomere lengths, much less force development is expected along the ascending limb of the cardiac length-tension relationship [2], [7], [19]. Second, the glue (silicone sealant) had an inherent compliance that could permit a fair amount of internal shortening in the cell. The amount of glue compliance varied from device to device since it was applied by hand. Additionally, the cell ends were not always optimally positioned in the clamps, which may result in partial cell slippage, striation pattern nonuniformity, and reduced recorded force. However, attachment and compliance issues are being addressed by redesigning the microstructure to include stiffer beams and a triple-plate hinged clamp. Superior adhesives are also being identified.

Compared with other macrosize transducers, the MEMS transducer described in this report should provide up to two orders of magnitude improvement in fidelity in solution (13.3 KHz). This improvement in fidelity is achieved without compromising sensitivity or noise levels. The overall performance of these MEMS devices will enable more sophisticated oscillatory stiffness or force/length transient analyzes to be performed on cardiac myocytes. Such studies can potentially reveal fundamental aspects of force generation and other mechanically related function in cells at the molecular level. With the important advances in molecular genetics and its relationship to cardiac diseases, such evaluations of simple cellular models like myocytes will assist in our fundamental understanding of heart function and dysfunction. Although a full range of studies were not performed here, the high-frequency data obtained from oscillating cardiac myocytes confirm that this new MEMS design permits cell measurements at higher fidelities than previously available with standard macro-transducers.

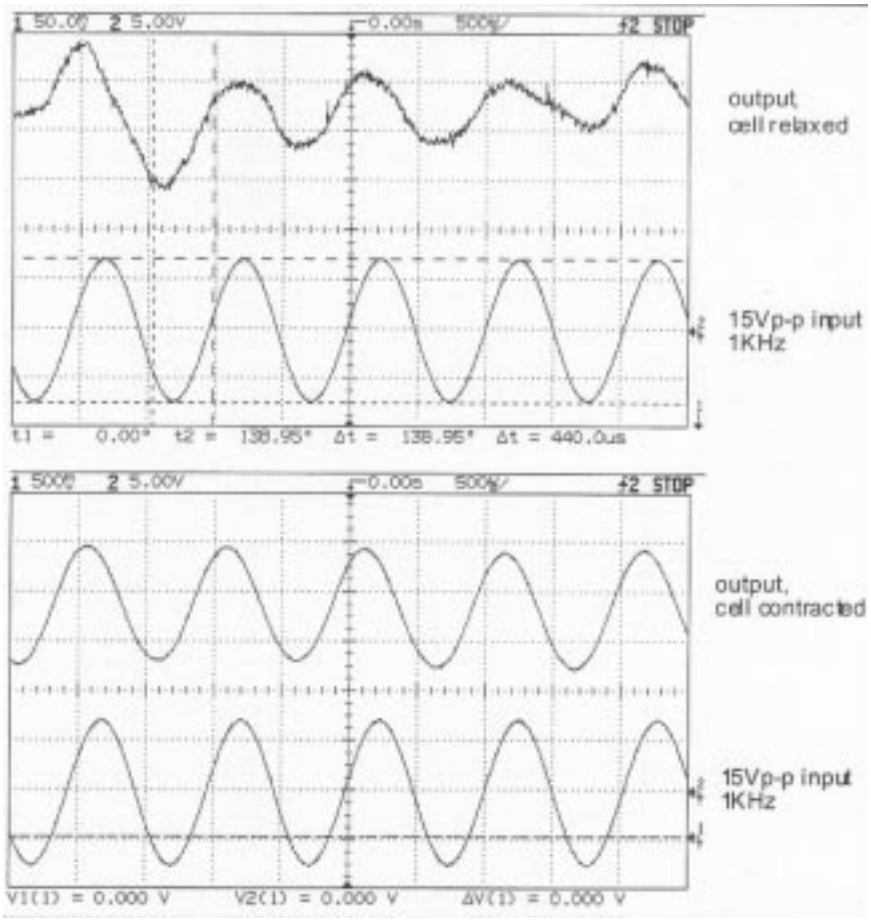

Fig. 12. Oscillatory force data. The voltage scaling for the relaxed cell force (upper pair) output is a factor of ten greater than for the activated cell (lower pair). These panels show recordings of the input voltage to the piezoelectric disk and the corresponding MEMS sensor output responses from a living cell oscillated at 1 KHz. The piezoelectric disk is attached to the clamp opposite the sensor bean. An increase in piezoelectric voltage (lower trace of each pair) moves this clamp toward the sensor clamp, thus shortening the cell. The upper trace of each pair is the MEMS transducer output voltage; an increase in voltage reflects sensor clamp movement toward the cell. Thus input peaks correspond to output valleys.

VI. Conclusion

The studies described above have utilized a disposable, fully submersible force transducer system implemented in MEMS technology specifically designed for use with a single, living heart cell. The scale of such devices is ideal for the study of many cell types or selected sub-cellular structures whose dimensions lie in the 25–250 μm range. This cell force transducer was successfully operated with cardiac myocytes in a saline bath surviving multiple solution exchanges under steady-state and oscillatory conditions. The fidelity of the data exceeds that previously achieved in a variety of cardiac myocyte studies published by others using macro-transducers [1], [4], [5], [14]. With a resonant bandwidth of 13 kHz in solution, this ultra-low mass device shows the potential for MEMS technology in the physiological assessment of mechanical forces in cardiac myocytes and other cell types under a wider variety of conditions and at higher fidelities than previously possible. Finally, such micromachined devices can be used to measure or probe a variety of cell types beyond force measurements from motile systems. These efforts could include the mechanical assessment of cytoskeletal components, mechanotransduction in intact or cultured cells, and simultaneous mechanical and electrophysiological measurement via integrated patch clamping.

Acknowledgment

The authors wish to thank J. Parker for contributing his technical expertise, H. Grona for building the imaging microscope, and Dr. K. Shen for preparing the cells. The authors also wish to thank Dr. D. Lee and Dr. E. Homsher for their assistance with beam calibration, and R. Yeh for originally designing the double metal hinge.

References

[1] A. Araujo and J. W. Walker, "Kinetics of tension development in skinned cardiac myocytes measured by photorelease of Ca^{2+}," *Amer. J. Physiol. 267 (36)*, vol. 267, no. 36, pp. H1643–H1653, 1994.

[2] A. J. Brady, "Mechanical properties of isolated cardiac myocytes," *Physiol. Rev.*, vol. 71, pp. 413–428, 1991.

[3] D. Garnier, "Attachment procedures for mechanical manipulation of isolated cardiac myocytes: A challenge," *Cardiovasc. Res.*, vol. 28, pp. 1758–1764, 1994.

[4] P. A. Hofmann and J. H. Lange, "Effects of phosphorylation of troponin I and C protein on isometric tension and velocity of unloaded shortening in skinned single cardiac myocytes from rats," *Circulation Res.*, vol. 74, pp. 718–726, 1994.

[5] K. S. McDonald, M. R. Wolff, and R. L. Moss, "Force-velocity and power-load curves in rat skinned cardiac myocytes," *J. Physiol. (London)*, vol. 511, pp. 519–531, 1998.

[6] R. E. Palmer, A. J. Brady, and K. P. Roos, "Mechanical measurements from isolated cardiac myocytes using a pipette attachment system," *Amer. J. Physiology*, vol. 270, no. 39, pp. C697–C704, 1996.
[7] K. P. Roos, "Mechanics of force production," in *The Myocardium*, 2nd ed, G. A. Langer, Ed. San Diego, CA: Academic, 1997, ch. 6, pp. 235–323.
[8] K. P. Roos and A. J. Brady, "Stiffness and shortening changes in myofilament extracted rat cardiac myocytes," *Amer. J. Physiol.*, vol. 256, pp. H539–H551, 1989.
[9] ——, "Osmotic compression and stiffness changes in relaxed skinned rat cardiac myocytes in PVP-40 and dextran T-500," *Biophys. J.*, vol. 58, pp. 1273–1283, 1990.
[10] N. K. Sweitzer and R. L. Moss, "The effect of altered temperature on Ca^{2+}-sensitive force in permeabilized myocardium and skeletal muscle. Evidence for force dependence of thin filament activation," *J. Gen. Physiol.*, vol. 96, pp. 1220–1245, 1990.
[11] K. S. J. Pister, "Hinged polysilicon structures with integrated thin film transistors," in *Proc. IEEE Solid State Sensor Actuator Workshop*, Hilton Head, SC, 1992, pp. 136–139.
[12] T. Neumann, M. Fauver, and G. H. Pollack, "Elastic properties of isolated thick filament measured by nanofabricated cantilevers," *Biophys. J.*, vol. 75, pp. 938–947, 1998.
[13] M. E. Fauver, D. L. Dunaway, D. H. Lilienfeld, H. G. Craighead, and G. H. Pollack, "Microfabricated cantilevers for measurement of subcellular and molecular forces," *IEEE Trans. Biomed. Eng.*, vol. 45, pp. 891–898, July 1998.
[14] C. Tasche, E. Meyhofer, and B. Brenner, "A force transducer for measuring mechanical properties of single cardiac myocytes," *Amer. J. Physiol.*, vol. 277, no. 46, pp. H2400–H2408, 1999.
[15] G. Lin, K. S. J. Pister, and K. P. Roos, "Micro-scale force transducer system to quantify isolated heart cell contractile characteristics," *Sensors Actuators A*, vol. 46, pp. 233–236, 1995.
[16] ——, "Surface micromachined polysilicon heart cell force transducer," *J. Microelectromech. Syst.*, vol. 9, no. 1, pp. 9–17, March 2000.
[17] ——, "Standard CMOS piezoresistive sensor to quantify heart cell contractile forces," in *Proc. IEEE MEMS-96 Workshop on Micro Electro Mechanical Systems*, San Diego, CA, 1996, pp. 150–155.
[18] G. Lin, R. E. Palmer, K. S. J. Pister, and K. P. Roos, "Single heart cell force measured in standard CMOS," in *Tech. Dig. Int. Conf. Solid-State Sensors and Actuators (Transducers '97)*, Chicago, IL, June 16–19, 1997, pp. 199–200.
[19] A. F. Huxley, "Review lecture: muscular contraction," *J. Physiol. (Lond.)*, vol. 243, pp. 1–43, 1974.
[20] W. C. Young, *Roark's Formulas for Stress and Strain*, 6th ed. New York: McGraw-Hill, 1989.
[21] K. E. Petersen, "Silicon as a mechanical material," *Proc. IEEE*, vol. 70, pp. 420–457, May 1982.
[22] J. L. Meriam and L. G. Kraige, *Engineering Mechanics: Dynamics*, 2nd ed. New York: Wiley, 1986.
[23] P. A. Tipler, *Physics*, 2nd ed. New York: Worth, 1982.
[24] P. J. French and A. G. R. Evans, "Polycrystalline silicon strain sensors," *Sensors Actuators (A)*, vol. 8, pp. 219–225, 1985.
[25] P. Horowitz and W. Hill, *The Art of Electronics*, 2nd ed. Cambridge, U.K.: Cambridge Univ. Press, 1989.
[26] P. R. Gray and R. G. Meyer, *Analysis and Design of Analog Integrated Circuits*, 2nd ed. New York: Wiley, 1984.
[27] Orbit Semiconductor's 2.0 μm (CMOS) process via the Metal–Oxide–Semiconductor Implementation Service. MOSIS - USC/Information Sciences Institute, Marina Del Rey, CA. [Online]. Available: http://www.mosis.org/
[28] P. B. Chu, J. T. Chen, R. Yeh, G. Lin, J. C. P. Huang, B. A. Warneke, and K. S. J. Pister, "Controlled pulse-etching with xenon difluoride," in *Dig. Tech. Int. Conf. Solid-State Sensors and Actuators (Transducers '97)*, Chicago, IL, June 16–19, 1997, pp. 665–668.
[29] E. Hoffman, B. Warneke, E. J. J. Kruglick, J. Weigold, and K. S. J. Pister, "3D structures with piezoresistive standard CMOS," in *Proc. IEEE MEMS-95 Workshop on Micro Electro Mechanical Systems*, Amsterdam, The Netherlands, 1995, pp. 288–293.
[30] K. P. Roos and S. R. Taylor, "High-speed video imaging and digital analysis of microscopic features in contracting striated muscle cells," *Opt. Eng.*, vol. 32, pp. 306–313, 1993.
[31] N. C. MacDonald, L. Y. Chen, J. J. Yao, Z. L. Zhang, J. A. McMillan, and D. C. Thomas, "Selective chemical vapor deposition of tungsten for microelectromechanical structures," *Sensors Actuators (A)*, vol. 20, pp. 123–133, 1989.

Gisela Lin received the B.S. degrees in electrical engineering and material science engineering from the University of California at Berkeley in 1990, the M.S. degree in electrical engineering from the University of California at Santa Barbara in 1992, and the Ph.D. degree in electrical engineering from the University of California at Los Angeles in 1998.

In 1998, she became a Member of the Technical Staff in the MEMS group at the NASA Jet Propulsion Laboratory, Pasadena, CA, where her research focused on MEMS biosensor packaging and the development of miniature immersible diagnostic systems. In 2000, she joined the Sales and Marketing Team at Standard MEMS, Inc., Hauppauge, NY, where she is currently a Technical Sales Engineer.

Roy E. Palmer received the D.Phil. degree from Oxford University, Oxford, U.K., in 1992 in the field of muscle physiology.

From 1992 until 1998, he was a Postdoctoral Research Fellow in the Cardiovascular Research Laboratory at the University of California School of Medicine, Los Angeles. He founded the medical website, TheDailyApple.com, and is currently Vice President of Products and Services for Caresoft Inc., Sunnyvale, CA.

Kristofer S. J. Pister received the B.A. degree in applied physics from the University of California at San Diego in 1982, and the M.S. and Ph.D. in electrical engineering from the University of California at Berkeley in 1989 and 1992.

In 1992, he became an Assistant Professor of Electrical Engineering at the University of California at Los Angeles where he developed three graduate-level courses in micro electro mechanical systems (MEMS): MEMS device physics and fabrication, MEMS design, and CAD for MEMS. In 1996, he joined the faculty of Electrical Engineering and Computer Sciences at the University of California at Berkeley as an Associate Professor. During the last five years, his primary research interest has been the development and use of standard fabrication technologies, general purpose design paradigms, and CAD for MEMS. Some of the applications of his research include micro robotics, micro optics, and distributed sensor networks. He is an active consultant in the MEMS industry, and has two patents on MEMS technology and applications.

Kenneth P. Roos received the A.B. degree in applied physics and information sciences from the University of California at San Diego in 1971, the M.S. degree in biology from San Diego State University in 1974, and the Ph.D. degree in zoology from the University of California at Davis in 1978.

He is with the Cardiovascular Research Laboratory and the Department of Physiology at the University of California at Los Angeles School of Medicine. He is currently an Adjunct Professor of Physiology and the Director of the Mouse Physiology Laboratory. His research interests focus upon the assessment of heart muscle contraction from the whole organ to the cellular level using novel biophysical and engineering approaches.

Dr. Roos is a member of the American Physiological Society, the Biophysical Society, the Cardiac Muscle Society, and the International Society for Heart Research. He is a Fellow of the American Heart Association.